Energy management of a hybrid system based on a fuel cell and a Lithium Ion battery: Experimental tests and integrated optimal design

A. Jaafar, C. Turpin, Xavier Roboam, E. Bru, O. Rallieres

Energy management of a hybrid system based on a fuel cell and a Lithium Ion battery: experimental tests and integrated optimal design

A. Jaafar[1], C. Turpin[1], X. Roboam[1], E. Bru[1], O. Rallieres[1]

1. Université de Toulouse, LAPLACE UMR CNRS–INP–UPS, ENSEEIHT 2, Rue Charles Camichel 31071 Toulouse, France.
e-mail: jaafar, turpin, roboam, bru, rallieres@laplace.univ-tlse.fr

Abstract

The optimal design of multisource systems, hybrid systems in particular, requires an adequate choice of the energy management strategy. This latter usually impacts source sizing and lifetime. The present paper deals with an energy management approach based on a frequency sharing of the mission. Firstly, the limits of a symmetric frequency energy management are presented in the case of a hybrid system associating a fuel cell with a Li-Ion battery. Subsequently, an original energy "asymmetric" management strategy for the optimal sizing of this association is presented. This strategy is then tested on the "Hydrogen" platform at the LAPLACE research laboratory. Finally, the two energy management strategies are compared in the context of an integrated design by optimization; the asymmetric strategy offers significant gains in terms of system weight, which is important for embedded applications.

Keywords: Fuel Cell, Battery, Lithium Ion, Energy Management Strategy, Optimal Design

Nomenclature

FC: Fuel Cell
BAT: Battery
SFEM: Symmetric Frequency Energy Management
AFEM: Asymmetric Frequency Energy Management
F_g: cutoff frequency of the low pass filter (used for SFEM)
W_g: cutoff pulsation of the low pass filter
*Fg*1: cutoff frequency used during the positive current gradient phases.
*Fg*2: cutoff frequency used during the negative current gradient phases.
I_BAT: battery current
I_FC: fuel cell current
I_load: load current
Ich_BAT: battery charge current
Ich_nom: nominal battery charge current

SOC: battery state of charge
I_HF: high frequency part of the load current
η_{act}: fuel cell activation losses
η_{diff}: fuel cell diffusion losses
R_{elec}: fuel cell internal resistance (ohmic losses)
E_{rev}: fuel cell reversible potential
N_{PBAT}: number of battery blocks in parallel
N_{SBAT}: number of battery cells in series
r_{BAT}: battery resistance
e_{BAT}: battery electromotive force
v_{BAT}: battery cell voltage
q_{BAT}: battery cell charge quantity
C: battery nominal capacity
i_{BAT}: battery cell current
$N_{b//\text{-}BAT}$: number of interleaved battery converter branches
$F_{d\text{-}BAT}$: battery converter switching frequency
$V_{stack\text{-}\min}$: fuel cell stack minimum voltage
$J_{FC\text{-}\max}$: fuel cell maximum current density
$F_{d\text{-}FC}$: fuel cell stack converter switching frequency
$N_{b//\text{-}FC}$: number of interleaved fuel cell stack converter branches
$P_{disch\_BAT\_\max}$: maximum discharge power that the battery can provide
$P_{disch\_profileBAT\_\max}$: maximum discharge power of the battery profile
$P_{ch\_BAT\_\max}$: maximum charge power authorized by the battery
$P_{ch\_profileBAT\_\max}$: maximum charge power of the battery profile
E_{tot}: stored energy in the battery
E_u: energy required to fulfill the battery profile
$DOD_{\max}$: maximum battery depth of discharge
N_{FC}: *number of fuel cells in series*
F_1: system weight
F_2: total losses energy

1. Introduction

Considering major energy challenges of this new century and in the context of fossil fuel depletion and greenhouse gas emissions, hydrogen is a promising solution for the storage of renewable energies and can be seen as “a potential energy vector for the future” [26]. Its transformation into electrical energy is ensured by a Fuel Cell (FC). Unlike storage components (batteries, ultra-capacitors, flywheels) where energy and power are closely linked in the same component, FCs offer energy / power decoupling. FC system can then be considered as an energy source (with a high specific energy range with respect to the

batteries) whose autonomy is related to the hydrogen tank size. As a consequence, the delivered power only depends on FC stack sizing.

Therefore, fuel cells are utilised in a wide range of applications, particularly in transport or embedded systems [7], [10] where weight and volume constraints are the key drivers, but also in stationary field [18] for which cost and efficiency are more concerned. In all these fields of application, the lifetime of such devices is also questioned and may be greater than 10,000 hours for constant operation. However, as soon as the electrical power draw becomes intermittent, the FC lifetime is significantly reduced. To overcome this difficulty, major applications rely on the hybridization of sources associating the FC with storage devices, while also defining an energy management strategy which optimizes power sharing between the FC and storage devices. In [6], [20], [14] and [12], authors have studied FC based hybrid structures with management strategies for electric vehicle applications; a double hybridization of FC source with ultra-capacitors and batteries is proposed in [32]. FC powered hybrid systems have also been studied for railway traction applications [22] or in more electric aircraft [17]; in this field of application, system weight has to be minimized as proposed in this paper. In [23], authors propose an original direct association of fuel cell devices with ultra-capacitor storage without any power electronic interface; the issue is here to enhance the life duration of fuel cells by means of this direct hybridization.

In order to associate efficiently several sources in a hybrid system, various types of energy management strategies can be applied. For example, “slope power sharing” [11], “band power sharing” [6], fuzzy logic based power sharing [20], [25], “optimal planning” based power sharing [28], [35], [15] and “frequency power sharing” [9], [17], [19] may be referred to.

In the present paper, we have studied and compared two energy management strategies, each of them being based on a frequency approach; this kind of strategy is applied to a particular hybrid system composed of a Fuel Cell device connected to a Li-Ion battery system. Classically, a Symmetric Frequency Energy Management (SFEM, described in sub section 2.1) is proposed as power management strategy; its main characteristic is related to the symmetry of power profile drawn from the storage device, limiting therefore the decrease of *SOC* during the system operation [33]. However, contrarily to the case of ultra-capacitor storage, the limitation of the SFEM strategy is mainly due to the asymmetry of charge vs discharge current capacities for Lithium Ion storage technologies. This asymmetry may lead to an oversizing of the storage device in order to be able to accept maximum charge current constraints then increasing the system weight. Due to this drawback, the SFEM has been

compared with an original management strategy called « Asymmetric Frequency Energy Management » (AFEM) which is specific to the Fuel Cell – lithium Ion storage association. Indeed, the asymmetry of charge/discharge current constraints on the accumulator is in accordance with the asymmetrical capabilities of fuel cell systems as described in sub section 2.2. The AFEM strategy is compared with the previous one by simulations (section 3) and has been experimentally tested on the « Hydrogen » platform of the LAPLACE lab as presented in section 4.

In the last section, an optimal design of the hybrid association integrating both (SFEM AFEM) strategies is proposed. This approach is especially dedicated to the field of embedded systems, especially for more electric aircraft for which geometrical constraints are the key issue. The system weight is then targeted as the most important design objective to be minimized together with system losses. Finally, the advantages of this original asymmetrical energy management strategy on the system weight are assessed in the context of a systemic design approach by optimization.

2. Energy management of the hybrid system

2.1. Symmetric frequency energy management

"Frequency" energy management is based on satisfying energy and power constraints of each source given its specific power/energy capability. It ensures the compatibility between the frequency components of the mission and the intrinsic frequency capacities of the different sources. In the case of the studied hybrid system, Symmetric Frequency Energy Management (SFEM) consists in providing the low frequency part of the mission by the FC. The high frequency part of the mission is then devoted to the battery. The implementation of this energy management strategy is rather simple and consists in using a low pass filter as shown in Figure 1. We denote by *Fg* the cutoff frequency of the filter.

Figure 2 illustrates the principle of SFEM. The variables *I_BAT* and *I_FC* represent the mission parts respectively sent to the battery and to the FC. *Wg* denotes the cutoff pulsation of the low pass filter ($Wg = 2\pi Fg$).

Let us note that this management strategy based on a frequency sharing does not manage regenerative load currents. Indeed, the FC system being non power reversible, potential regenerative currents should be necessarily accepted by the battery. Consequently, the battery profile would not remain symmetric. This issue has to be taken into account for electric

vehicle application. However, our privileged class of systems deals with embedded systems as for aircraft electric networks for which only positive global power consumption are considered.

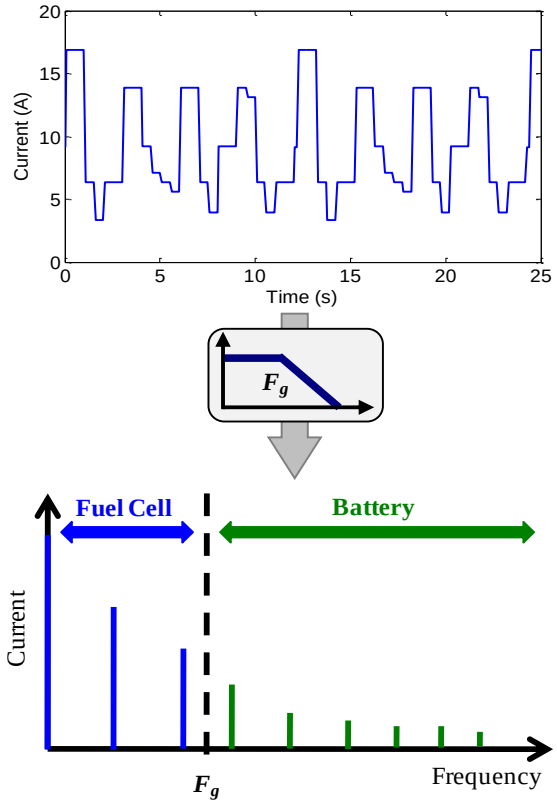

Fig. 1. Crossing between mission and source power sharing: (top graph: time chronogram of the mission profile, lower graph: frequency current sharing plan)

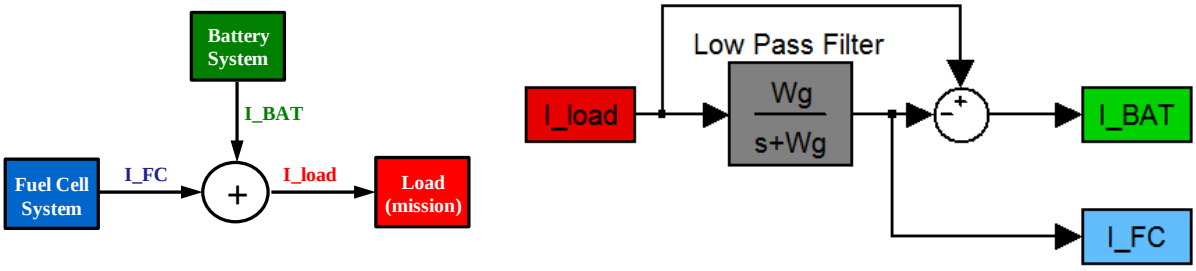

Fig. 2. Principle of Symmetric Frequency Energy Management

Figure 3.a shows an example of frequency sharing applied to an "academic" mission (square wave) with a cutoff frequency F_g = 0.5 Hz. The FC provides the low frequency part of

the mission (*I_FC*) and the battery provides the high frequency part (*I_BAT*). We can observe that according to the sign convention chosen in the study, positive currents correspond to discharge while negative currents deal with charge phases.

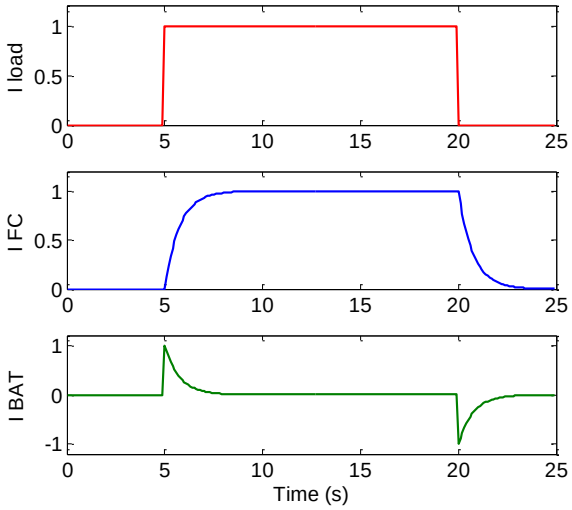

Fig. 3.a. Illustration of Symmetric Frequency Energy Management

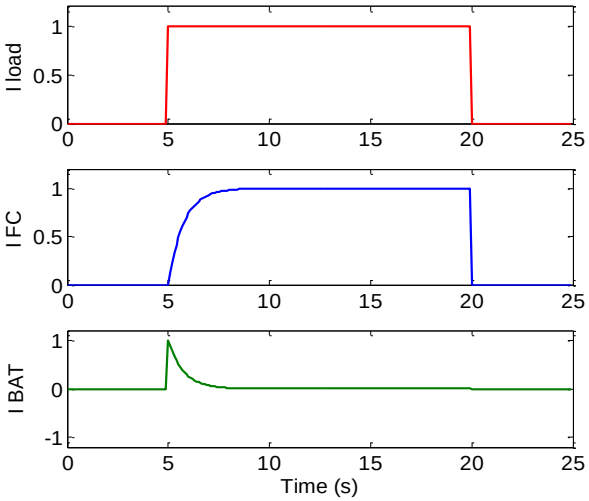

Fig. 3.b. Illustration of Asymmetric Frequency Energy Management

The battery mission profile (*I_BAT*) obtained in Figure 3.a shows that the charge phases have the same maximum current (in absolute value) as the discharge phases. Furthermore, based on the symmetry of charge vs discharge phases, this mission is characterized by a low energy content (simply due to the storage system losses) compared to the energy required for the global load mission (*I_load*). This symmetry of charge vs discharge phases has two main consequences:

-On the one hand, only losses in the battery – the chopper – the cable association have to be compensated as these latter provoke a very slow decrease of the battery SOC. A supplementary current (*Ich_BAT*) has to be provided by the fuel cell to compensate this slow decrease. Several strategies are possible to control the battery *SOC* or to limit its slow decrease as explained in [17] for a fuel cell – ultra capacitor hybrid system. As illustrated on Figure 4, a battery recharging open loop control may be added. Note that this compensation loop has not actually been implemented in experiments based on SFEM strategy. Indeed, during the time interval of the mission profile (less than 4 hours) the very slow decrease of *SOC* (only due to losses) makes unnecessary to implement the *SOC* compensation loop.

-On the other hand, considering the natural dissymmetry between the Li Ion battery charge and discharge current capacities (conversely to the case of ultra-capacitors), the sizing of the storage device is clearly constrained by the charge current. For example, the manufacturer of our Li-Ion battery recommends a maximum discharge current of 90 A and a maximum charge current of only 6 A. Consequently, the battery necessary to satisfy the *I_BAT* mission is oversized in terms of energy and power. This is solely due to the maximum charge currents; this issue is emphasized in section 5 where optimal design constraints are studied. To solve this problem, in the next section a proposal related to Asymmetric Frequency Energy Management strategy (AFEM) is outlined.

2.2. Asymmetric frequency energy management

Asymmetric Frequency Energy Management (AFEM) principle implies providing the low frequency part of the mission by the FC as for SFEM, but only during phases characterized by a positive gradient of current. Subsequently, the battery provides a discharge current which corresponds to the rest of the mission, i.e., the high frequency components of the mission power during positive gradients. Conversely, the battery is not charged during the negative gradient of the mission profile, this load being fully achieved by the FC system.

For the positive gradients, the major risk for the FC is the gas starvation during the transitory periods due to the time response of the gas supplies [5], [24], [34]. So, because of too small gas flows during these transient periods, the carbon electrodes will be a little bit consumed (CO_2 production). By repeating a lot of times the positive gradients, the degradation of the electrodes is then accelerated.

For the negative gradients, the major risk could be the membrane drying due to the time response of the gas supplies again (the gas flows are too high during the transient periods) but the time constant for the drying is more than several minutes, so this drying phenomenon cannot occur in practice [3], [16]. The negative gradients are then not degrading for the FC.

According to this energy management strategy, the mission of the battery would not include charge currents. Consequently, contrarily to the SFEM case, the battery charge would not naturally be ensured. A battery slow charging loop respecting manufacturer's recommendations should be added. The battery may be charged with a current (*Ich_BAT*) which varies linearly according to its state of charge (*SOC*) as shown in Figure 4. However, if the battery state of charge is lower than a minimum threshold (SOC_{min}), the battery charge is

ensured at the nominal charge current (*Ich_nom*). In the case where the battery state of charge exceeds a maximum threshold (SOC_{max}), the battery charge is disabled.

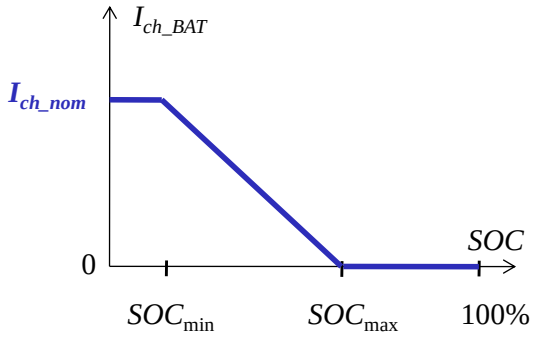

Fig. 4. The principle of the battery recharging loop

The block diagram of AFEM is given in Figure 5. A low pass filter is used to determine the low frequency part of the mission. Practically, in order to overcome discontinuity problems in the FC mission (*I_FC*), two cutoff frequencies are attribuated to the low-pass filter. The first frequency (*Fg*1) is used during the positive current gradient phases. The second (*Fg*2) is only used during the negative current gradient phases. It should be noted that the *Fg*2 frequency should be higher than the first frequency (*Fg*1) so that the output of the low pass filter nearly follows the initial mission (*I_load*) during the negative current gradient phases, as quickly as possible.

Thus, as illustrated on the synoptic of Figure 5 for AFEM strategy, a first part of the FC mission (*I_FC0*) is equal to the low frequency part of the load mission (*I_LF*) obtained with the frequency switching between (*Fg*1) and (*Fg*2) following the sign of the load current gradient. A second part of the FC mission is related to the ‘’Battery current charge loop’’ block. This latter block allows maintaining the battery *SOC* despite the battery system losses and the asymmetry of the mission profile. This same battery current charge (*Ich_BAT*) is deducted from the initial battery mission (*I_HF*).

Note that in the case of symmetric energy management strategy, the unique cut-off frequency *Fg* represents a degree of freedom (both the FC profile and battery profile are sensitive to this frequency) which affects both fuel cell and storage sizing. In the context of an integrated optimal design, this frequency is considered as an optimization parameter.

In the case of asymmetric energy management strategy, the cut-off frequency Fg_1 is determined in the same way (by optimization) as the cut-off frequency *Fg* in the case of symmetric energy management strategy. It is necessary that the cut-off frequency Fg_2 is high

enough to deal with fast dynamics of the load profile during negative gradients. In the case of the profile under study, it has been set to 100 Hz with regard to the capacity of the FC current controller bandwidth.

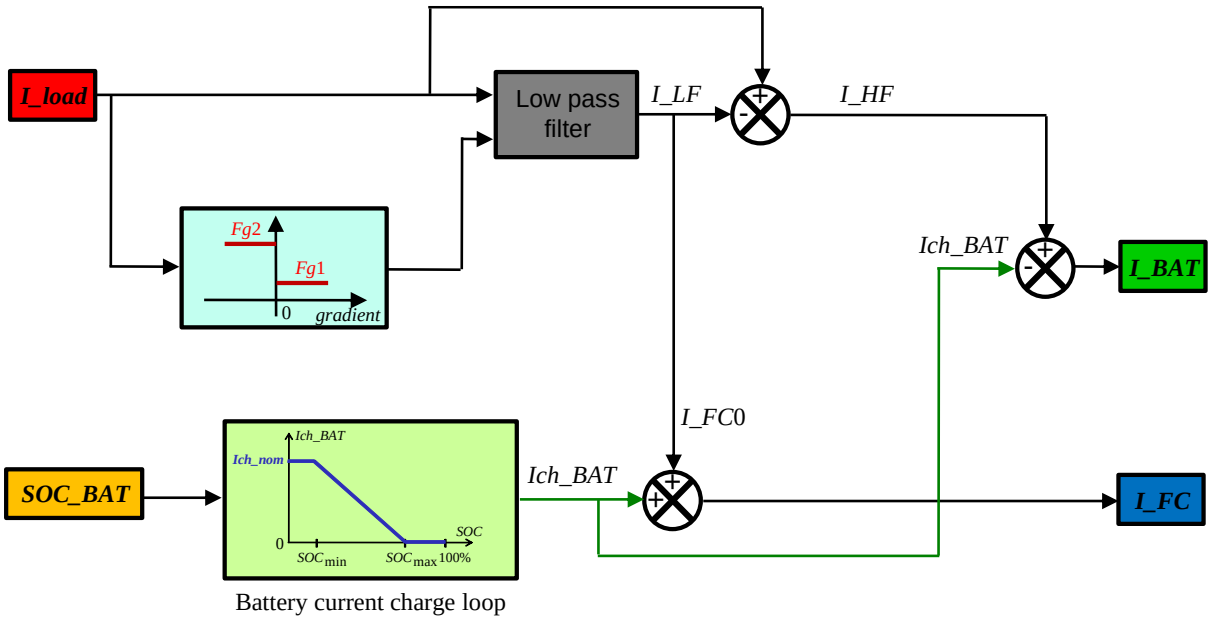

Fig. 5. Principle of the Asymmetric Frequency Energy Management

Figure 3.b illustrates the principle of AFEM with a cutoff frequency $Fg1 = 0.5$ Hz. To simplify the analysis, the case considered is where the battery state of charge is higher than the maximum threshold (SOC_{max}). The battery current charge loop is then disabled ($Ich\_BAT = 0$).

It should be noted that only a simplified system vision has been put forward in this section in order to emphasize the comparative performance of both (SFEM vs AFEM) management strategies. Thus, current controllers have not been described as being composed of classical structures. In reality, these controllers are necessary to control currents and also to limit current peaks during transients. However, these constraints are not so drastic due to the relatively slow dynamics of the practical mission profile. Furthermore, these control loops have been implemented in experiments discussed in section 4.

Finally, as for the SFEM, it is also true that regenerative currents would set constraints on battery charge currents even with the AFEM, leading to a storage oversizing. However, as for our case study, except to the hybrid vehicle case, a wide class of embedded systems does not require managing regenerative powers; it is for example the case of aircraft systems for which the load profile does not contain energy recovery phases (negative charge power). This

application field is in fact our main target but this issue has not been emphasized due to generality concern of our talk.

3. The simulation of the hybrid system

In this section, the simulation results of the hybrid system with both energy management strategies are presented. The simulation software used in this study is Matlab Simulink.

The hybrid system simulation is based on quasi-static electrical models as illustrated on Figure 6. According to our scientific experience [27], [30], the global energy behavior at system level is quasi equivalent whatever dynamic electrical models with control loops or quasi-static electrical models with ideal current controllers are used. This remark is valid only if current controller bandwidths are rapid enough to deal with the reference dynamics, which is the case in our study due to the medium dynamics on the mission profile. As an example, dynamics displayed in Figure 3 (i.e some seconds of time range) to illustrate power management issues are quite slow with respect to current controller time responses (i.e some milliseconds of the time range). This model simplification is also validated through our experimental study (Figure 11) which suggests the same behavior of the hybrid system in terms of current sharing between battery and fuel cell devices. Experimentally, we have also obtained a good bus voltage quality and stability (Figure 12) which proves that voltage/current controllers are sufficiently fast to be idealized at the hybrid system level, making relevant the assumption of quasi-static electrical models.

The fuel cell quasi-static electrical model takes into account the activation (η_{act}), ohmic ($R_{elec} \times I_{FC}$) and diffusion (η_{diff}) losses. The fuel cell voltage is obtained by subtracting the total losses from the reversible potential E_{rev} as shown in Figure 6.a.

The input of this model is the current *I_FC* stemming from energy management strategies given in Figure 2 or Figure 5.

Concerning the battery quasi-static electrical model, a *R, E* electrical model is used to obtain the battery cell voltage v_{BAT}. The input of this model is the current *I_BAT* stemming from energy management strategies given in Figure 2 or Figure 5. The cell current is obtained by dividing *I_BAT* by the number of battery blocks in parallel (N_{PBAT}).

The battery resistance r_{BAT} and its electromotive force e_{BAT} are interpolated from manufacturer's data according to the cell state of charge (*SOC*). The battery *SOC* is obtained from the ratio of the cell charge quantity (q_{BAT}) to its nominal capacity (*C*). The charge quantity (q_{BAT}) is defined as the sum of the integral of the cell current (i_{BAT}) and the initial

charge quantity of the cell (q_0). According to the sign convention, the battery discharge current is considered to be positive.

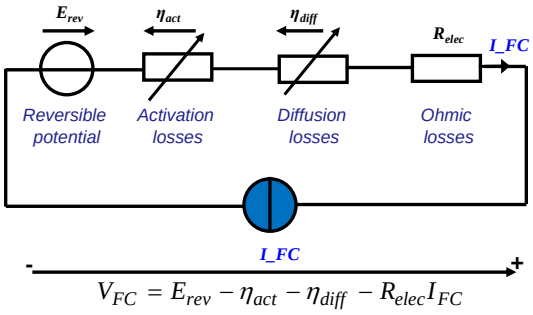

Fig. 6.a. Fuel cell quasi-static electrical model

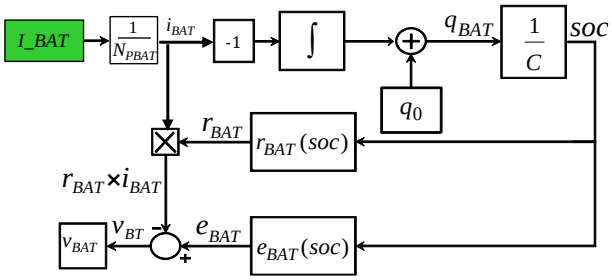

Fig. 6.b. Battery cell quasi-static electrical model

The simulated profile (*I_load*) corresponds to the actual load profile to be fulfilled by the hybrid system. A cycle of 12 s (Figure 7) is continously repeated.

Figure 7.a shows simulation results of the hybrid system with SFEM. The cutoff frequency is fixed at 0.3 Hz. This value is compatible with the response-time of an H_2/O_2 FC system selected for the tests in question. Verification was carried out to ensure that the FC provides the low frequency part of the mission while the battery provides the rest (i.e the high frequency part).

It should be remembered that in the present study, the hybrid system topology shown in Figure 8 was initially sized. This system is composed of a 5 kW H_2/O_2 FC stack with a Li-Ion battery characterized by a nominal voltage of 216 V and a nominal capacity of 6 Ah (the series connection of 60 accumulator cells with a nominal voltage of 3.6 V). As recommended by the manufacturer (due to ageing issues), the battery may be solicited during discharge with a maximum current of 15 C (90 A) and with a maximum charge current of 1 C (6 A). Under such conditions, the 216 V battery is unable to satisfy the current profile *I_BAT* shown in Figure 7.a. Indeed, the charge current (the negative part of the curve) strongly exceeds, in absolute value, the nominal charge current (6 A). In order to satisfy this frequency sharing of the mission, one solution is to use two 216 V batteries in parallel. This solution obviously leads to a significant weight increase.

Unlike SFEM, the mission sharing according to AFEM fully respects the source sizing. In fact, Figure 7.b shows that the battery charge current (the negative part of *I_BAT*) does not exceed the nominal charge current (*Ich_nom* = 6 A). It can be observed that the level of the battery charge current depends only on the battery state of charge. Some of the dynamic

constraints (strong negative current gradients for the *I_FC* in Figure 7.b) are transferred on the FC *a priori* without any impact on its lifetime. Further aging tests are forecast to confirm this assessment.

We verify in Figure 7.b that the FC guarantees the low frequency part of the mission only during the positive current gradient phases. It also ensures the battery charge current.

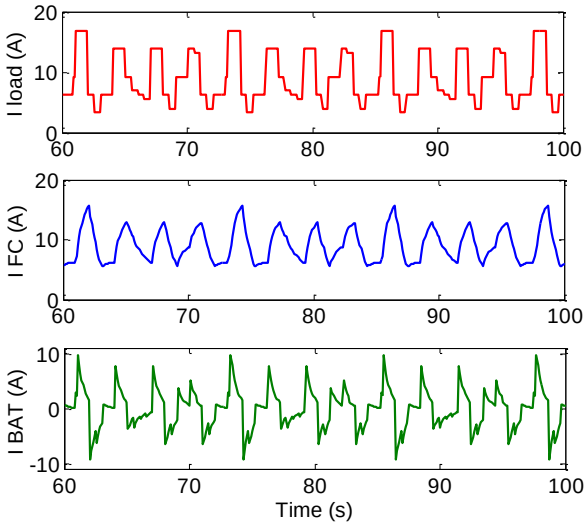

Fig. 7.a. Simulation of the mission profile with Symmetric Frequency Energy Management

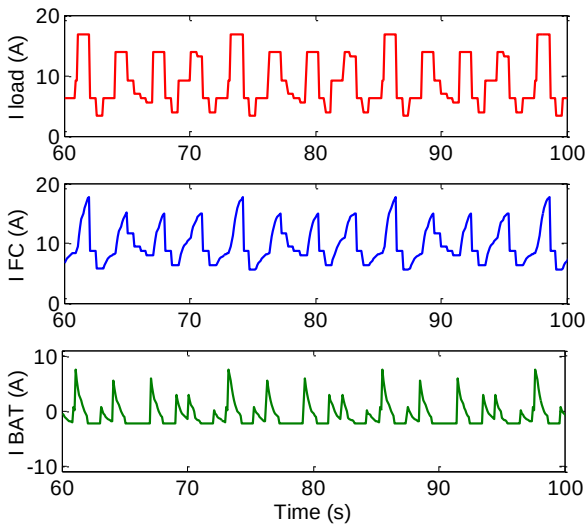

Fig. 7.b Simulation of the mission profile with Asymmetric Frequency Energy Management

4. Experimental results

As previously mentioned, the LAPLACE laboratory is equipped with a ‘’Hydrogen’’ platform with facilities used here for testing a 5 kW H_2/O_2 FC stack with a 216 V Li-Ion battery. Both sources are connected to a 270 V HVDC bus through two DC/DC power converters (Figure 8); it should be noted that the 270 V DC bus is called “HVDC” in the aeronautic field (which is our main application target) contrary to low voltage DC for 28 V avionic loads. The test bench structure ‘’FC-Li-ion Battery Hybridization’’ is illustrated in Figure 8 with some pictures of devices in Figure 9.

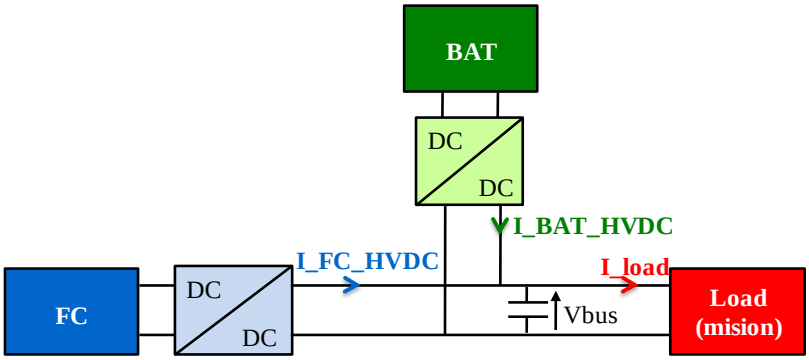

Fig. 8. The architecture of the experimental test bench

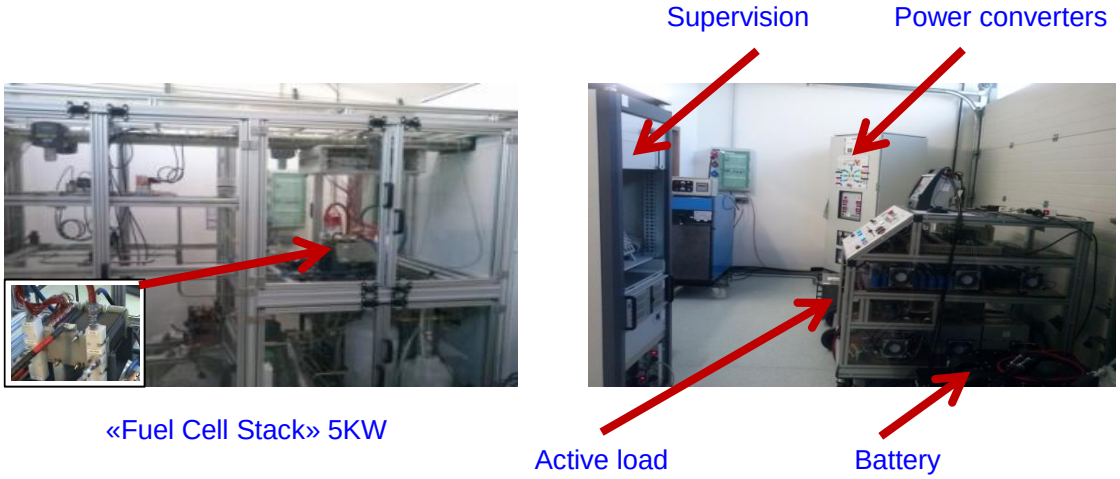

Fig. 9. The ‘’FC-Li-ion Battery Hybridization’' test bench on the « Hydrogen » platform of the LAPLACE laboratory

In this section, only experiments on AFEM strategy are presented. The complete load profile given in Figure 10 represents a typical operation case of the hybrid system with a duration of 2 hours and 42 minutes. During the first five minutes, the battery provides the entire load profile and the fuel cell stack is not yet activated. When $t \in [1\text{ min}, 5\text{ min}]$, the battery provides also the required power of the fuel cell stack auxiliaries. The current consumed by the fuel cell stack auxiliaries is estimated at 2 A. The hybridization starts at $t = 5$ min.

Figure 10 shows also the evolution of the battery *SOC*. In the first 5 minutes, the battery *SOC* decreases rapidly from 100% to 81%. In fact, during this period, the battery is the only available power source of the hybrid system. The battery recharging loop is not yet active. At $t = 5$ minutes, the hybridization starts and the battery recharging loop is activated which allows maintaining the battery *SOC* around 60%. At $t = 2$ hours and 42 minutes, the

hybridization stops. However the fuel cell continues to charge the battery according to the principle of Figure 4.

The losses in the fuel cell power converter are compensated by the fuel cell by producing an additional power resulting in H_2 and O_2 over-consumption. Concerning the battery system losses (battery losses + battery converter losses), a loss compensation loop is required to prevent the drift of the battery SOC. These losses are also supplied by the fuel cell. In the case of SFEM, the dynamic of the loss compensation loop should be slow regarding the fuel cell dynamic. In the case of AFEM, the loss compensation loop is integrated in the battery recharging loop. In both cases, the compensation of the battery system losses leads to H_2 and O_2 over-consumption.

The waveforms of both "HVDC bus side" FC and battery currents, respectively referred to as *I_FC_HVDC* and *I_BAT_HVDC*, and the load current *I_Load* at the HVDC bus are given in Figure 10 and Figure 11. The experimental results are perfectly in accordance with AFEM simulation results given also in Figure 10 and Figure 11 which contributes to validate the simulation modelling.

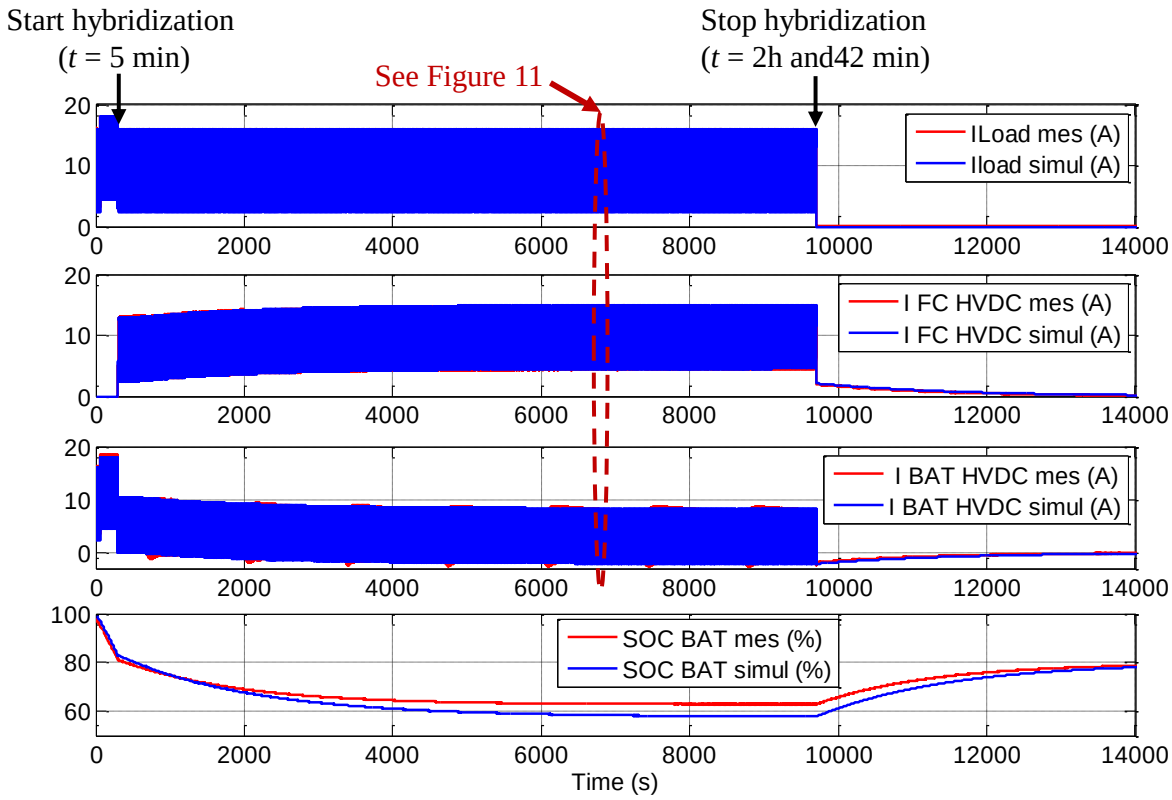

Fig. 10. The experimental and simulation results of Asymmetric Frequency Energy Management strategy

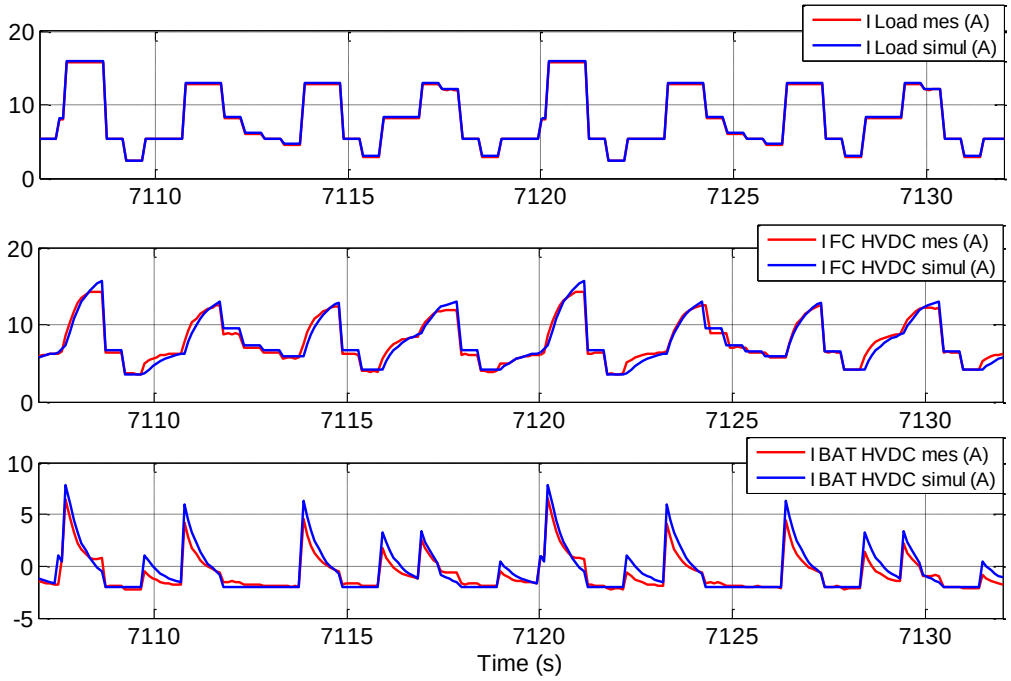

Fig. 11. Zoom of experimental and simulation results of Asymmetric Frequency Energy Management strategy

Figure 12 shows the experimental evolution of the DC bus voltage. This result shows a good bus voltage stability. This latter issue shows that voltage/current controller bandwidths are fast enough to face the load profile dynamics. In that particular case, the bus voltage has been regulated by the battery storage sub system while the FC sub system is current controlled by fulfilling the current sharing strategy as proposed in AFEM principle.

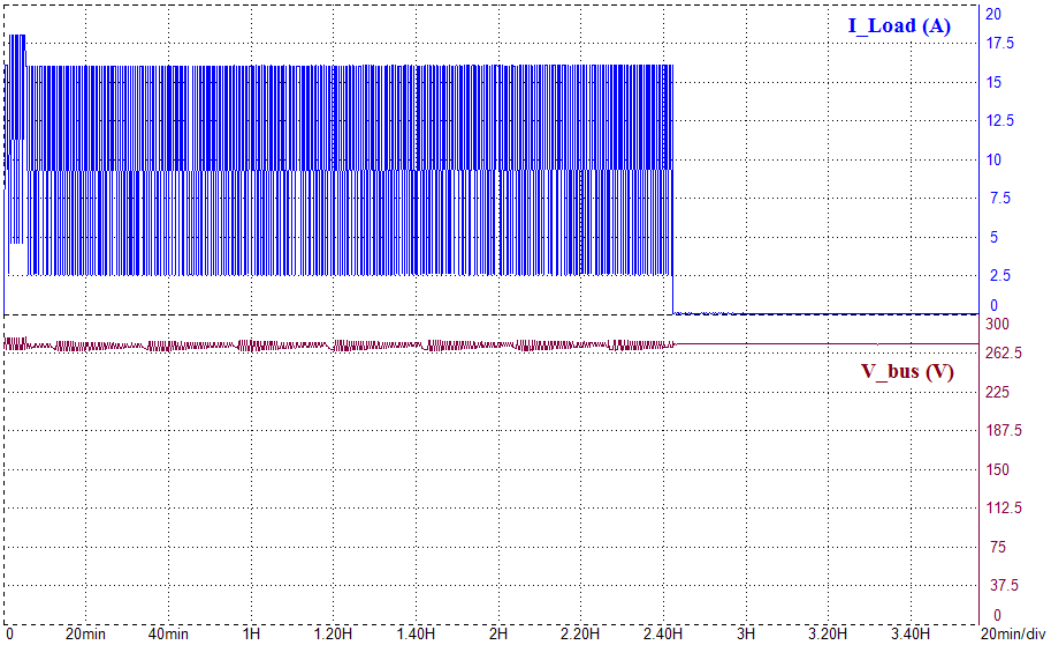

Fig. 12. The experimental evolution of the DC bus voltage

5. Comparison of the two energy management strategies in the context of optimal sizing of the hybrid system

In this section, the optimal design of the hybrid system is discussed; the optimized process is the one displayed in Figure 8. The objective of this design approach is to identify solutions with low weight and low losses.

5.1. The optimization process

The optimization process is given in Figure 13. A Non-dominated Sorting Genetic Algorithm (NSGA-II) [13], [31] is used to solve this two objective problem. This algorithm allows generating the design variables which are then injected into the hybrid system sizing model in order to evaluate the optimization criteria and constraints. The load current profile is an input for the simulation of the hybrid system model.

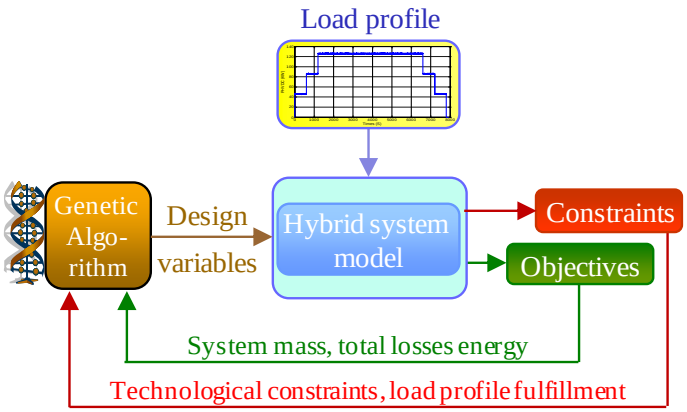

Fig. 13. Optimization process

5.2. The design variables

The design variables (here 9 variables) are illustrated in Figure 14 and are given in Table 1.

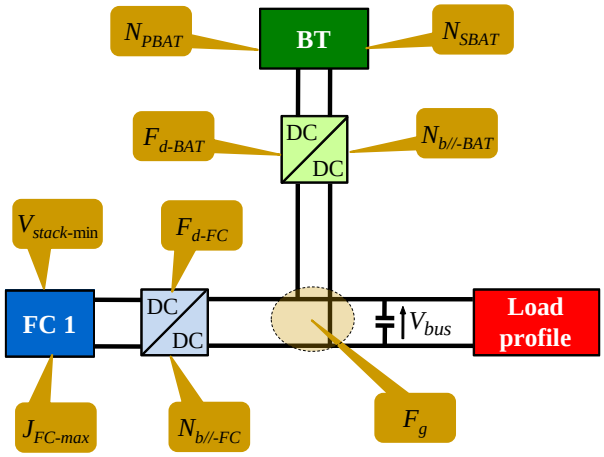

Fig. 14. *The illustration of design variables*

Table 1. *List of design variables*

Symbol	Design Variable
F_g	Power sharing frequency (the cutoff frequency of the low pass filter) $F_g = F_{g1}$ in the case of AFEM (F_{g2} being fixed at 100 Hz)
N_{SBAT}	Number of battery cells in series
N_{PBAT}	Number of battery blocks in parallel
$N_{b//\text{-}BAT}$	Number of interleaved battery converter branches
$F_{d\text{-}BAT}$	Battery converter switching frequency
$V_{stack\text{-min}}$	FC stack minimum voltage
$J_{FC\text{-max}}$	FC maximum current density
$F_{d\text{-}FC}$	FC stack converter switching frequency
$N_{b//\text{-}FC}$	Number of interleaved FC stack converter branches

With regard to the energy source sizing models (FC and battery), the reader is invited to consult [8], [17], [19] and [21]. The sizing model of the power converter is given in [29].

5.3. The design constraints

The optimization constraints are related to technological limitations of energy sources and to the satisfaction of the current sizing profile. Five inequality constraints formulated in terms of minimization (i.e. $g_i \leq 0$, $i = \{1,\ldots,5\}$) should be respected to guarantee the feasibility of the hybrid system.

As the number of battery cells is the product of two design variables ($N_{BAT} = N_{SBAT} \times N_{PBAT}$), the equivalent battery should provide a suitable response to some energy and power constraints:

- The maximum discharge power

  The maximum discharge power that the battery can provide ($P_{disch\_BAT\_\max}$) should be higher than or equal to the maximum discharge power of the battery profile ($P_{disch\_profileBAT\_\max}$).

$$g_1 = P_{disch\_profileBAT\_\max} - P_{disch\_BAT\_\max} \leq 0 \quad (1)$$

- The maximum charge power

  The maximum charge power authorized by the battery ($P_{ch\_BAT\_\max}$) should, in absolute value, be higher than or equal to the maximum charge power of the battery profile ($P_{ch\_profileBAT\_\max}$).

$$g_2 = \left| P_{ch\_profileBAT\_\max} \right| - \left| P_{ch\_BAT\_\max} \right| \leq 0 \quad (2)$$

- *The stored energy*

  The energy which can be stored in the battery (E_{tot}) should be higher than the energy required for the battery profile (E_u). İndeed, according to the manufacturer's recommendations, only a percentage of E_{tot} is allowed to satisfy a certain maximum Depth of Discharge ($DOD_{\max}$) [4]:

$$g_3 = E_u - DOD_{\max} \times E_{tot} \leq 0 \quad (3)$$

Concerning the FC stacks, the constraints are:

- *The number of FC cells in series*

  For structural reasons and gas distribution problems, the number of FC cells in series is limited to 300 [36], [37]:

$$g_4 = N_{FC} - 300 \leq 0 \quad (4)$$

- *The FC surface*

  The FC surface is also subjected to technological constraints related to current density, uniform distribution of temperature and mechanical clamping forces. It is limited to 2500 cm^2:

$$g_5 = S_{FC} - 2500 \leq 0 \quad (5)$$

5.4. The design objectives

Two conflicting design objectives are considered in this study: the system weight F_1 and the energy of system losses F_2.

$$\begin{cases} F_1 = M_{FC} + M_{CV\text{-}FC} + M_{BAT} + M_{CV\text{-}BAT} + M_{H2} \\ F_2 = Losses_{FC} + Losses_{CV\text{-}FC} + Losses_{BAT} + Losses_{CV\text{-}BAT} \end{cases} \quad (6)$$

where M_{FC}, $M_{CV\text{-}FC}$, M_{BAT}, $M_{CV\text{-}BAT}$ respectively denote FC stack mass, FC power converter mass, battery mass and battery power converter mass. M_{H2} denotes the mass of hydrogen consumed during the mission and the mass of the corresponding tank. The stored hydrogen density is fixed to 5%: a 100 kg tank is needed to store 5 kg of H_2 [1].

The total losses energy F_2 is obtained by the time integral of the power loss in both energy sources (FC stack and battery) and power converters.

5.5. The optimization results

A comparison between the optimal sizing of the hybrid system with SFEM and that which is obtained with AFEM has been carried out. Both Pareto fronts are given in Figure 15. For confidentiality reasons, the results of Figure 15 are given in per-unit. It is clear that asymmetric frequency energy management (AFEM) strongly dominates symetric strategy (SFEM); it offers significant gain in terms of system weight compared to symmetric frequency energy management (SFEM).

Figure 16 shows the distribution of the system mass between the battery system (battery converter + battery) and the FC system (FC stack + FC converter + FC auxiliaries + H_2 tank). This difference between the two management strategies is mainly due to the batteries whose sizing constraints, in the case of SFEM, are due to the charge current: as recommended by the manufacturer the maximum battery charge current is equal to 1 C (6 A) to preserve life duration. Indeed, the battery mass represents approximately 70% of the system mass. The FC system mass is almost the same with the two energy management strategies (AFEM and SFEM).

It should be noted that in order to minimize the system losses, the optimizer tends to choose oversized fuel cell stacks. Indeed, from the energy point of view, a large-sized FC is more efficient than a small one.

By making the assumption that the battery can accept higher charge currents, a significant gain in terms of mass may be achieved compared to a charge current of only 1C. However, responding to fast charging phases may possibly deteriorate the battery lifetime.

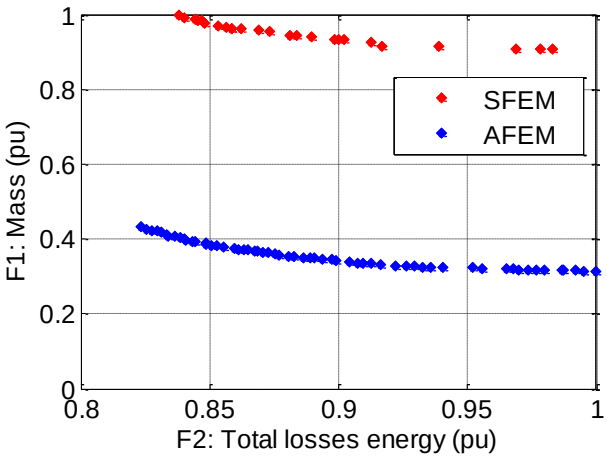

Fig. 15. Comparison of the two Pareto fronts obtained with symmetric and asymmetric energy management strategies

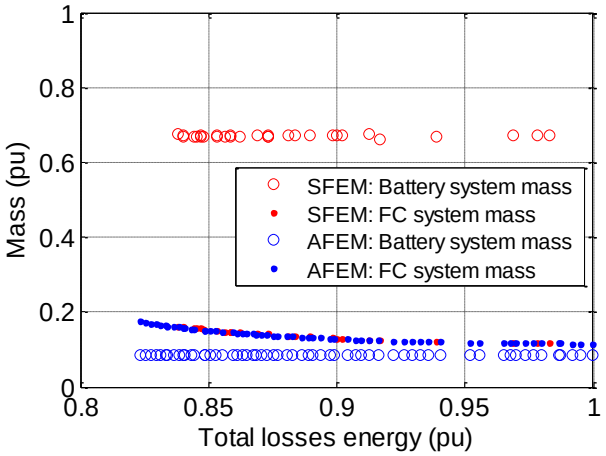

Fig. 16. The system mass distribution between the battery system (battery converter + battery) and the FC system (FC stack + FC converter + FC auxiliaries + H_2 tank)

6. Conclusion

In the present paper, two energy management strategies of an autonomous hybrid system based on the association of a Fuel Cell and a Li-Ion battery are presented. Both strategies are based on a frequency sharing of the mission; here the current profile which is related to the power sharing given the bus voltage. This frequency based strategy ensures compatibility between frequency components of the mission and intrinsic dynamical characteristics of sources, especially when the power profile is positive without regenerative phases; this kind of profile is usually required in various classes of embedded systems as in aircraft applications. Through simulations of a real (typical) mission of the hybrid system, the authors have shown the interest of Asymmetric Frequency Energy Management compared to Symmetric Frequency Energy Management in terms of system sizing. A number of dynamical constraints is transferred to the FC; conclusive evidence related to the lack of lifetime impact is not yet available. As a following, experimental results of Asymmetric Frequency Energy Management are presented. Finally, the impact of the choice related to the energy management strategy on the hybrid system weight has been illustrated in the context of an integrated optimal design: this study confirms the interest of an original asymmetric strategy for this example of typical source association and in the framework of typical mission profiles.

References

[1] P. Adams, Identification of the optimum on-board storage pressure for gaseous hydrogen city buses, European integrated hydrogen project EIHP2 Report, Gothenburg Sweden, 2004.

[2] C.R. Akli, X. Roboam, B. Sareni, A. Jeunesse, Integrated optimal design of a hybrid locomotive with multiobjective genetic algorithms, Int. J. Appl. Electromagn. Mech., 30 (2009) 151–162.

[3] F. Barbir, H. Gorgun, X. Wang, Relationship between pressure drop and cell resistance as a diagnostic tool for PEM fuel cells, J. Power Sources, 141 (2005) 96–101.

[4] M. Belouda, A. Jaafar, B. Sareni, X. Roboam, J. Belhadj, Integrated optimal design and sensitivity analysis of a stand alone wind turbine system with storage for rural electrification, Renew. & Sustain. Energy Rev., 28 (2013) 616–624.

[5] R. Borup, J. Meyers, B. Pivovar, Y. S. Kim, R. Mukundan, N. Garland & al, Scientific Aspects of Polymer Electrolyte Fuel Cell Durability and Degradation, Chem. Rev, 107 (2007) 3904–3951.

[6] F.N. Büchi, A. Delfino, P. Dietrich, S.A. Freunberger, R. Kötz, & al., Electrical Drivetrain Concept with Fuel Cell System and Supercapacitor Results of the "HYLIGHT®"-vehicle, VDI Tagung Innovative Fahrzeugantriebe, Dresden, Germany, 2006, pp. 415–426.

[7] C. C. Chan, The State of the Art of Electric, Hybrid, and Fuel Cell Vehicles, Proc. of the IEEE., 95 (2007) 704–718.

[8] W. Chanpeng, Y. Khunatorn, B. Plangklang, Model and experiment analysis of 1.2 kW PEMFC electrification, Proced. Eng., 8 (2009) 106–114.

[9] P. Chapoulie, S. Astier, Modelling of an Electric Vehicle Including Ultracapacitors with SABER, Vehicle Symposium and Exposition Conf., Bruxelles, Belgium, 1998.

[10] M. A .J. Cropper, S. Geiger, D.M. Jollie, Fuel Cells: A survey of current developments, J. of Power Sources, 131 (2004) 57–61.

[11] V. Dang Bang, Y. Lembeye, J. P. Ferrieux, J. Barbaroux, New high power - high ratio non isolated DC-DC boost converter for Fuel cell applications, IEEE Power Electronics Specialists Conf., 2006, pp. 1–7.

[12] B. Davat, S. Astier, T. Azib, O. Bethoux, O. Candusso, G. Coquery, A. De Bernardinis, F. Druart, B. François, M.G. Arreguy, F. Harel, D. Hissel, J.P. Martin, M.C. Pera, S. Pierfederici, S. Rael, D. Riu, S. Sailler, Y. Bultel, T. Creuzet, C. Turpin, T. Zhou, Fuel cell-based hybrid systems, Electromotion Conf, Lille, France, 2009.

[13] K. Deb, S. Agrawal, A. Pratab, T. Meyarivan, A fast-elitist non-dominated sorting genetic algorithm for multiobjective optimization: NSGA–II, Proc. of the Parallel Problem Solving from Nature VI Conf., Athens, Greece, 2000, pp 849–858.

[14] A. Drolia, P. Jose, N Mohan, An approach to connect ultracapacitor to fuel cell powered electric vehicle and emulating fuel cell electrical characteristic, using switched mode converter, Industrial Electronics Society, IECON '03, 1(2003) 897–901.

[15] D. Feroldi, M. Serra, J. Riera, Energy Management Strategies based on efficiency map for Fuel Cell Hybrid Vehicles, J. Power Sources, 190 (2009) 387–401.

[16] N. Fouquet, C. Doulet, C. Nouillant, G. Dauphin-Tanguy, B. Ould-Bouamama, Model based PEM fuel cell state-of-health monitoring via ac impedance measurements, J. Power Sources, 159 (2006) 905–913.

[17] M. Garcia Arregui, Theoretical study of a power generation unit based on the hybridization of a fuel cell stack and ultracapacitors, Ph.D. Thesis, Institute National Polytechnique, Toulouse, 2007. Available from URL: http://ethesis.inp-toulouse.fr/archive/00000521/.

[18] J. Hamelin, K. Agbossou, A. Laperrière, F. Laurencelle, T. K. Bose, Dynamic behavior of a PEM fuel cell stack for stationary applications, Int. J. Hydrog. Energy, 26 (2001) 625–629.

[19] A. Jaafar, C. Akli, B. Sareni, X. Roboam, A. Jeunesse, Sizing and energy management of a hybrid locomotive based on flywheel and accumulators, IEEE Trans. Veh. Technol., 58 (2009) 3947–3958.

[20] J. S. Martínez, D. Hissel, M. C. Péra, M. Amiet, Practical Control Structure and Energy Management of a Test bed Hybrid Electric Vehicle, IEEE Trans. Veh. Technol., 60 (2011) 4139–4152.

[21] L. Menard, G. Fontes, S. Astier, Dynamic Energy Model of a Lithium-Ion battery, Math. Comput. Simul., 81 (2010) 327–339.

[22] A.R. Miller, K.S. Hess, D.L. Barnes, T.L. Erickson, System design of a large fuel cell hybrid locomotive, J. Power Sources, 173 (2007) 935–942.

[23] B. Morin, D. Van Laethem, C. Turpin, O. Rallières, S. Astier, A. Jaafar, O. Verdu, M. Plantevin, V. Chaudron, Direct hybridization of Fuel cell – Ultracapacitors, Fundamentals & Development of Fuel Cells Conf., Karlsruhe, Germany, 2013, pp. 500–507.

[24] R. Lin, F. Xiong, W.C. Tang, L. Técher, J.M. Zhang, J.X. Ma, Investigation of dynamic driving cycle effect on the degradation of proton exchange membrane fuel cell by segmented cell technology, J. Power Sources, 260 (2014) 150–158.

[25] C. N. Papadimitriou, N. A. Vovos, Integration of a hybrid fuel cell-battery system to a distribution grid, Electr. Power Syst. Res., 81 (2011) 1299–1307.

[26] M.C. Péra, H. Gualous, D. Hissel, C. Turpin, Electrochemical components, ISTE Ltd, London, John Wiley & Sons, New York, 2013.

[27] K. Rafal, B. Morin, E. Bru, X. Roboam, C. Turpin, H. Piquet, Experimental Validation of Hybrid Emergency Electrical Network for Aircraft Application, IEEE VPPC Conf., Lille, France, 2010, pp 1–6.

[28] F. Rajaei, Control Strategies for Hybrid Electric Vehicles: Evolution, Classification, Comparison, and Future Trends, IEEE Trans. Veh. Technol., 56 (2007) 2393–2404.

[29] R. Rigo Mariani, F. Lacressonniere, G. Fontes, X. Roboam, Design of a medium voltage power converter storage devices embedded in a hybrid emergency network for more electrical aircraft, Math. Comput. Simul., 91 (2013) 72–90.

[30] X. Roboam, S. Astier, Y. Besanger, E. Bideaux, A. Bouscayrol, G. Dauphin-Tanguy & al, Systemic Design Methodologies for Electrical Energy Systems: Analysis, synthesis and management, ISTE Ltd, London, John Wiley & Sons, New York, 2012.

[31] B. Sareni, L. Krahenbuhl, Fitness sharing and niching methods revisited, IEEE Trans. Evol. Comput., 3 (1998) 97–106.

[32] P. Thounthong, S. Raël, B. Davat, Energy management of fuel cell/battery/supercapacitor hybrid power source for vehicle applications, J. Power Sources, 193 (2009) 376–385.

[33] C. Turpin, S. Astier, X. Roboam, B. Sareni, H. Piquet, Systemic Design Methodologies for Electrical Energy Systems, John Wiley & Sons, London, 2012, pp. 223−283.

[34] N. Yousfi-Steiner, Ph. Moçotéguy, D. Candusso, D. Hissel, A review on polymer electrolyte membrane fuel cell catalyst degradation and starvation issues: Causes, consequences and diagnostic for mitigation, J. Power Sources, 194 (2009) 130–145.

[35] Y. Zhu, Y. Chen, G. Tian, H. Wu, Q. Chen, A four-step method to design an energy management strategy for hybrid vehicles, Proc. the American Control Conf., Boston, MA, USA, 2004, pp. 156–161.

[36] http://hydrogenics.com/, September 2014.

[37] http://www.ballard.com/, October 2014.